Journal of Solid State Chemistry 182 (2009) 3055–3062

Contents lists available at ScienceDirect

Journal of Solid State Chemistry

journal homepage: www.elsevier.com/locate/jssc

Crystal growth and magnetic behavior of $R_6T_{13-x}Al_xM_y$ phases (R = La, Nd; T = Mn, Fe; M = main group) grown from lanthanide-rich eutectic fluxes

Evan M. Benbow, Naresh S. Dalal, Susan E. Latturner *

Department of Chemistry and Biochemistry, Florida State University, Tallahassee, FL 32306, USA

ARTICLE INFO

Article history:
Received 14 June 2009
Received in revised form
7 August 2009
Accepted 8 August 2009
Available online 15 August 2009

Keywords:
Metal flux synthesis
$Nd_6Fe_{13}Si$ type
$La_6Co_{11}Ga_3$ structure
Magnetism
Type II antiferromagnetism
Iron layer
Manganese intermetallic

ABSTRACT

Binary eutectic mixtures of early lanthanide metals and late transition metals have been explored as media for crystal growth of new intermetallic phases. A large family of $R_6T_{13-x}Al_xM_y$ phases (R = La or Nd; T = Fe or Mn; M = main group elements) with the $La_6Co_{11}Ga_3$ structure type can be crystallized from La/Ni and Nd/Fe eutectics. The tetragonal structure of these compounds features slabs of transition metal atoms capped with mixed T/Al sites and separated by layers of lanthanide ions. The growth of large crystals of the lanthanum analogs allows for the study of the anisotropic magnetic properties of the transition metal slabs. For $La_6Fe_{13-x}Al_xM_y$ analogs, these order antiferromagnetically with T_N strongly dependent on the Fe/Al ratio on the mixed sites. Growth of Mn analogs is reported for the first time; the transition metal slabs in $La_6(Mn/Ni)_{10}Al_3$ phases order ferromagnetically with a T_C of 200 K.

1. Introduction

Due to their high melting points, La (m.p. 918 °C) and Ni (m.p. 1455 °C) are not ideal elements for use as molten metal solvents (flux) to synthesize intermetallic products. However, when combined in an 88:12 wt% ratio they form a eutectic with a melting point of 532 °C [1]. This flux is being explored as a medium for the growth of new lanthanide phases. The use of molten metal solvents enhances diffusion of the reactants, provides a wide temperature range for single crystal growth, and allows isolation of products by means of centrifugation to remove the excess flux [2]. In many instances, these molten metals act not only as solvents, but also as reactants which are incorporated in the final product (i.e. reactive flux). The La/Ni metal eutectic flux is a unique system that combines a reactive component (lanthanum) with a largely inert component (nickel). We have crystallized numerous Fe-based intermetallics such as $La_{21}Fe_8M_7C_{12}$, $LaFe_{12}B_6$, and $R_6Fe_{13-x}M_{1+x}$ from this flux mixture without any Ni incorporation [3].

The magnetic, structural, and hydriding properties of $R_6Fe_{13-x}M_{1+x}$ (R = early lanthanide, M = Al, Ga, Si, Ge) with the $La_6Co_{11}Ga_3$-type tetragonal structure (in space group $I4/mcm$) have attracted the interest of many research groups [4–6]. The structure, shown in Fig. 1, consists of iron slabs separated by layers comprised of R and M, stacked along the c-axis. The binary variant of this phase (R_6Fe_{14}) does not exist; a third element is required to mix into the $16l_2$ and $4a$ sites to stabilize the structure (resulting in ternary variants such as $La_6Fe_{13-x}Al_{1+x}$); we have found that a fourth more electronegative element can be incorporated in the $4a$ site to create quaternary analogs such as $La_6Fe_{10}Al_3P_1$. Much of the focus has been on the $Nd_6Fe_{13}Si$ variant due to its presence as an impurity phase which can enhance coercivity in Nd–Fe–B permanent magnets [7]. Few studies have been performed on La analogs, and most studies are hindered by the inability to synthesize single crystals of these peritectic phases using traditional synthetic techniques and the common occurrence of impurities such as α-Fe, La_2Fe_{17}, and La_3Al [8].

In this work, large single crystals of $La_6Fe_{13-x}Al_xM_y$ analogs have been grown from La/Ni eutectic. The structural variations with the identity of M and the filling of the mixed and partially occupied sites have been explored and may prove crucial to understanding and tailoring the magnetic properties of these phases. We have also investigated Nd/Fe and La/Mn eutectics to crystallize additional $R_6T_{13-x}Al_xM_y$ analogs, isolating manganese-containing phases for the first time. All the members of this family exhibit either temperature- or field-induced magnetic phase transitions and are attractive systems for applications in materials science and for the study of fundamental magnetic properties such as itinerant-electron magnetism (IEM). The magnetic properties of these $R_6Fe_{13-x}M_{1+x}$ compounds are controversial with various magnetic ordering models being proposed, based on

* Corresponding author. Fax: +1 850 644 8281.
E-mail addresses: ebenbow@chem.fsu.edu (E.M. Benbow), dalal@chem.fsu.edu (N.S. Dalal), latturne@chem.fsu.edu (S.E. Latturner).

0022-4596/$ - see front matter © 2009 Elsevier Inc. All rights reserved.
doi:10.1016/j.jssc.2009.08.011

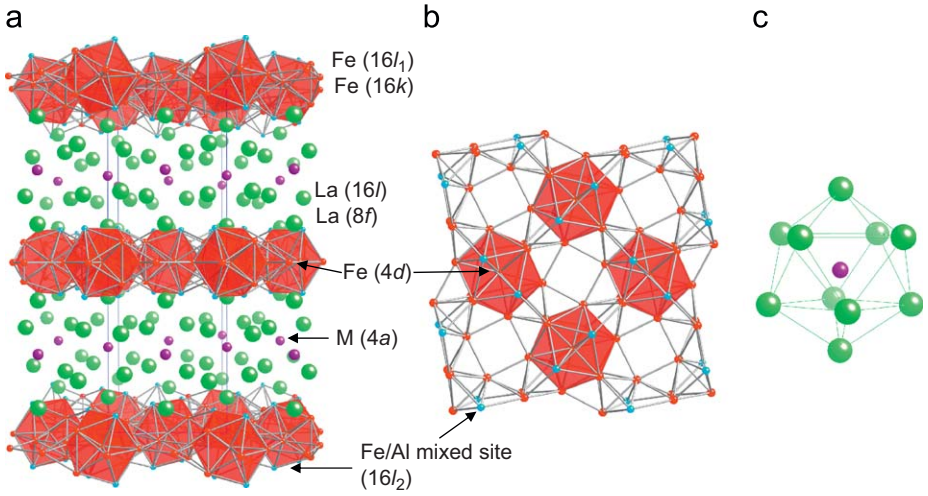

Fig. 1. (a) The tetragonal structure of $R_6Fe_{13-x}Al_xM_y$ compounds, viewed down the *a*-axis. (b) The transition metal slab, comprised of linked icosahedra, viewed down the *c*-axis. (c) The local environment of the 4*a* site (occupied by main group element).

competing intralayer and interlayer ordering mechanisms [9]. The exploration of the La analogs is crucial to isolating the behavior of the iron layers in the absence of magnetic moments in the lanthanide layers.

2. Experimental procedure

2.1. Synthesis

Starting materials for preparation of $La_6Fe_{13-x}Al_xM_y$ phases were powders of the lanthanide metals La or Nd (METALL Rare Earth Ltd and Acros, purity >99.9%), powders of Fe, Bi, Sb, (Strem Chemicals, 99.9%), Cu, Au, P (Alfa Aesar >99.9%), Ag (Premlon >99.9%), Ge (Cerac >99.9%), chips of Pb (Fisher Scientific >99.7%), and In (Alfa Aesar >99.9%). Chips cut from ingots of La/Ni eutectic (88:12 wt%, Alfa Aesar 99.9%, m.p. 532 °C) were used for the flux reagent. The standard reactant amounts were 1.0 mmol of La, 1.5 mmol Fe, 0.5 mmol Al and 0.3 mmol of main group element *M* layered between ~1 g of La/Ni flux in an alumina crucible. This was placed in a fused silica tube; another alumina crucible was filled with silica wool, inverted and placed on top of the reaction crucible to act as a filter during centrifugation. The silica tube was then sealed under a vacuum of 10^{-2} Torr. Various heating profiles were investigated (*vide infra*), but the best results were obtained by heating to 950 °C in 3 h, holding at this temperature for 12 h, then cooling to 850 °C in 10 h. The samples were then annealed for 48 h at 850 °C then cooled to 600 °C in 84 h. At 600 °C the fused silica ampoules were then removed from the furnace, inverted and quickly placed into a centrifuge to remove excess molten flux.

Due to the high lanthanum content, the La/Ni eutectic flux is an aggressive reducing agent that will leach Al from alumina crucibles; this resulted in our initial synthesis of the $La_{6-}Fe_{13-x}Al_xM_y$ phases. The reactivity of the flux also provides a useful way to remove any residual flux coating remaining on the crystals by leaving the products out overnight. The La-rich flux oxidizes in air, and the product crystals can be picked out of the lanthanum oxide/nickel powder. This allows isolation of the product without using etching solvents which could damage the crystals. Due to the layered growth habit of this system, any remaining flux on the surface can be removed by shearing off a small layer of the crystal using a scalpel if scraping is not successful. The crystals are sufficiently stable to allow extended handling in air, but were stored in a dry box as a precaution to prevent any degradation.

2.2. Elemental analysis

Elemental analysis was performed on all samples using a JEOL 5900 scanning electron microscope with energy dispersive spectroscopy (SEM–EDS) capabilities. Samples were analyzed using a 30 kV accelerating voltage and an accumulation time of 40 s. To avoid interference from possible traces of residual flux coating on the surface of the crystals, they were broken and scans were taken on the interior fragments. Analysis of crystals typically showed ratios for the La, Fe, Al, and M in agreement with those observed in the XRD structure solution. Because of the possibility of nickel contamination from the flux the samples were also monitored for this element; it was not observed in any of the scans of $La_6Fe_{13-x}Al_xM_y$ products, but small amounts of Ni were indicated in the $La_6Mn_{13-x}Al_xM_y$ crystals (*vide infra*).

2.3. X-ray diffraction

After analysis by EDS to determine the composition of the large flux-grown crystals, small interior shards were cleaved from the crystals. The shards were mounted on glass fibers using epoxy, and single-crystal X-ray diffraction data for each compound were collected at room temperature on a Bruker AXS SMART CCD diffractometer. Data processing was then performed using the program SAINT; an absorption correction was applied to the data using the SADABS program [10]. The structure was solved using direct methods and refined with the SHELXTL package of programs [11]. Unit cell parameters and mixed and partial site occupancies for the compounds studied here can be found in Tables 1 and 2; crystallographic collection parameters for three representative compounds are listed in Table 3. Further details of the crystal structure investigations can be obtained from the Fachinformationszentrum Karlsruhe, 76344 Eggenstein-Leopoldshafen, Germany (e-mail: crysdata@fiz.karlsruhe.de) on quoting the registry numbers CSD 420883 to 420907.

2.4. Magnetic susceptibility

Magnetic susceptibility measurements were performed with a Quantum Design MPMS SQUID magnetometer at temperatures between 1.8 and 400 K. Anisotropic measurements were

Table 1
Unit cell parameters and mixed site occupancies for ternary $R_6T_{13-x}Al_{1+x}$ compounds (R = La or Nd; T = Fe or Mn) grown in La/Ni or Nd/Fe flux.

Compound	T occupancy of $16l_2$ site[a]	T occupancy of $4a$ site[a]	a (Å)	c (Å)	R_1[b]
$La_6Fe_{10.5}Al_{3.5}$	0.34(1)	0.11(2)	8.2168(4)	23.699(2)	0.0291
$La_6Fe_{10.4}Al_{3.6}$	0.27(1)	0.35(2)	8.2297(3)	23.792(2)	0.0257
$La_6Fe_{10.4}Al_{3.6}$	0.32(2)	0.15(3)	8.2352(4)	23.790(3)	0.0352
$La_6Fe_{10.4}Al_{3.6}$	0.315(9)	0.09(1)	8.2294(4)	23.768(3)	0.0193
$La_6Fe_{10.3}Al_{3.7}$	0.30(1)	0.09(3)	8.2268(3)	23.773(2)	0.0355
$La_6Fe_{10.2}Al_{3.8}$	0.29(1)	0.08(3)	8.2368(7)	23.800(4)	0.0328
$La_6Fe_{10.1}Al_{3.9}$	0.27(1)	0.04(3)	8.2342(4)	23.777(2)	0.0283
$La_6Fe_{10.1}Al_{3.9}$	0.24(2)	0.09(4)	8.2365(6)	23.750(3)	0.0424
$La_6Fe_{10}Al_4$	0.23(1)	0.03(3)	8.238(1)	23.704(7)	0.0268
$La_6Mn_{10}Al_4$	0.21(1)	0.15(3)	8.4533(3)	23.935(2)	0.0285
$Nd_6Fe_{11}Al_3$	0.49(1)	0.01(2)	8.1335(7)	23.103(4)	0.0206
$Nd_6Fe_{10.5}Al_{3.5}$	0.367(9)	0.01(2)	8.1513(6)	23.141(3)	0.0197

[a] Occupancy of $16l_2$ and $4a$ sites refined as mixed T/Al.
[b] $R_1 = \Sigma|(|F_o|-|F_c|)|/\Sigma|F_o|$, for $I>2\sigma(I)$ data.

Table 2
Unit cell parameters and site occupancies for $R_6T_{13-x}Al_xM_y$ quaternary compounds synthesized in La/Ni flux.

Compound	T occupancy of $16l_2$ site[a]	M occupancy of $4a$ site[b]	a (Å)	c (Å)	R_1[c]
$La_6Fe_{9.8}Al_{3.2}P_1$	0.21(1)	1.01(2)	8.2408(3)	23.748(2)	0.0230
$La_6Fe_{9.9}Al_{3.1}S_{0.92}$	0.21(2)	0.91(3)	8.2394(5)	23.759(2)	0.0403
$La_6Fe_{10.2}Al_{2.8}Cu_{0.49}$	0.29(1)	0.49(1)	8.2227(3)	23.699(2)	0.0359
$La_6Fe_{10.5}Al_{2.5}Ge_{0.74}$	0.37(1)	0.74(1)	8.212(1)	23.642(1)	0.0316
$La_6Fe_{9.9}Al_{3.1}As_1$	0.23(1)	1.00(1)	8.254(1)	23.868(7)	0.0302
$La_6Fe_{10.2}Al_{2.8}Se_{0.37}$	0.31(1)	0.37(1)	8.223(1)	23.666(5)	0.0263
$La_6Fe_{9.8}Al_{3.2}Ag_{0.66}$	0.21(2)	0.66(1)	8.2498(7)	23.781(4)	0.0435
$La_6Fe_{9.8}Al_{3.2}Sb_{0.92}$	0.21(1)	0.917(6)	8.2583(2)	23.8653(8)	0.0243
$La_6Fe_{10.1}Al_{2.9}Au_{0.22}$	0.29(1)	0.220(4)	8.2296(3)	23.711(2)	0.0247
$La_6Fe_{10.4}Al_{2.6}Pb_{0.65}$	0.36(1)	0.644(3)	8.2368(2)	23.925(1)	0.0226
$La_6Fe_{9.4}Al_{3.6}Bi_{0.47}$	0.09(3)	0.465(9)	8.2695(4)	23.902(2)	0.0445
$La_6Fe_{10.1}Al_{2.9}Bi_{0.75}$	0.26(2)	0.753(8)	8.2752(9)	23.984(5)	0.0389
$La_6Fe_{9.5}Al_{3.5}Bi_{0.91}$	0.125(11)	0.909(4)	8.2842(4)	24.037(3)	0.0218
$La_6Mn_{10.5}Al_{2.5}Sb_{0.91}$	0.38(1)	0.909(5)	8.4175(6)	23.951(3)	0.0213
$Nd_6Fe_{11.5}Al_{1.5}Sb_{0.5}$	0.62(2)	0.50(1)	8.1144(3)	23.116(1)	0.0314

[a] Occupancy of $16l_2$ site refined as mixed T/Al.
[b] The $4a$ site refined as partially occupied by the M element.
[c] $R_1 = \Sigma|(|F_o|-|F_c|)|/\Sigma|F_o|$, for $I>2\sigma(I)$ data.

Table 3
Crystallographic data and structure refinement parameters for three representative $R_6T_{13-x}Al_{1+x}$ ternary compounds.

	$La_6Fe_{10.5}Al_{3.5}$	$La_6Mn_{10}Al_4$	$Nd_6Fe_{10.5}Al_{3.5}$
Formula weight (g/mol)	1514.26	1489.78	1545.72
Space group	*I*4/*mcm*	I4/*mcm*	*I*4/*mcm*
a (Å)	8.2168(4)	8.4533(3)	8.1513(6)
c (Å)	23.699(2)	23.934(2)	23.141(3)
V (Å^3)	1600.0(2)	1710.3(2)	1537.6(3)
d_{calc} (g/cm^3)	6.285	5.786	6.677
Z	4	4	4
Temperature (K)	293	293	293
Radiation	Mo$K\alpha$	Mo$K\alpha$	Mo$K\alpha$
$2\theta_{max}$	56.59	56.56	56.64
Index ranges	$-10\le h\le 10$	$-11\le h\le 11$	$-10\le h\le 10$
	$-10\le k\le 10$	$-11\le k\le 11$	$-10\le k\le 10$
	$-31\le l\le 31$	$-31\le l\le 31$	$-30\le l\le 30$
Reflections collected	11045	11674	10670
Unique data/parameters	566/36	597/35	548/36
μ (mm^{-1})	24.55	21.87	29.08
R_1/wR_2 [$I>2\sigma(I)$][a]	0.0291/0.0563	0.0285/0.0581	0.0197/0.0411
R_1/wR_2 (all data)[a]	0.0291/0.0563	0.0286/0.0582	0.0198/0.0411
Residual peak/hole (e/Å^3)	1.310/−1.233	5.206/−0.851	1.542/−0.942

[a] $R_1 = \Sigma|(|F_o|-|F_c|)|/\Sigma|F_o|$; w$R_2 = (\Sigma w[(F_o^2-F_c^2)^2]/\Sigma w[(F_o^2)^2])^{1/2}$.

performed on single crystals sealed in kapton tape and rigidly secured within the sample holder in specific orientations with respect to the applied field. Field cooled and zero-field cooled temperature dependence measurements were collected at 0.2 T, and field dependent measurements from 0 to 7 T were collected at 1.8 K.

3. Results and discussion

The facility with which crystals of iron-rich intermetallics can be grown from a commercially available La/Ni eutectic has led to the crystallization of a wide range of ternary $La_6Fe_{13-x}Al_{1+x}$ and quaternary $La_6Fe_{13-x}Al_xM_y$ compounds, listed in Tables 1 and 2, respectively. This allows investigation of the effects of stoichiometry variation on the structure, and also facilitates the characterization of anisotropic magnetic behavior. We have also expanded the study of lanthanide/transition metal eutectic flux chemistry to the Nd/Fe and La/Mn systems to explore further variation of this structure type.

3.1. Synthesis

$La_6Fe_{13-x}Al_{1+x}$ is typically synthesized using traditional arc melting and annealing techniques yielding impure polycrystalline samples, although Canfield et al. have investigated growth of $Nd_6Fe_{13-x}Al_{1+x}$ in melts rich in Nd and Al relative to their desired product [12]. During our syntheses in La/Ni flux, the heating program was varied in attempts to increase crystal yield and size. Changes to dwell times and cooling rates had minimal effect on crystal growth. Changes in the initial ramping rate, on the other hand, had very noticeable results. Use of a quick initial ramp time of 3 h yielded the best results, with the molten flux easily centrifuged from the well-formed product crystals at the end of the reaction. Using a slower ramp rate seems to facilitate side reactions that scavenge some of the flux before it can melt and solvate the reactants; at the end of these reactions, little or no flux is observed to have separated from the products, which are usually in the form of polycrystalline chunks instead of large crystals.

3.1.1. Iron compounds

We are able to grow single crystals of a variety of iron-based intermetallics using the La/Ni flux, such as $LaFe_{12}B_6$, $La_6Fe_{13-x}Al_{1+x}$, $La_{3+d}FeC_6$, and a new compound $La_{21}Fe_8M_7C_{12}$ (M = Bi, Sb, Sn) [3,13]. All these structures feature iron clusters, layers, or networks interspersed with lanthanide ions. SEM–EDS elemental analysis of the crystal interiors showed no incorporation of Ni into any of the Fe-based intermetallics discussed above. Refinement of crystallographic data also showed no indication of a heavier element in the Fe sites. It appears that the presence of iron in the reaction mixture causes the nickel in the solvent eutectic to behave as an inert flux—an element that serves to dissolve the reactants, but is not incorporated into the products. Many examples of inert flux behavior have been reported, such as the growth of Si and Ge phases (including $CrSi_2$, WSi_2, RSi_2, and α-$RNiGe_2$) using indium as a flux, and the growth of a wide variety of lanthanide transition metal phosphides from tin flux [2]. If iron is not present in the reaction or is present in small amounts, the nickel in the flux becomes reactive; for instance, crystals of $La_5Ni_{2-d}Si_3$ and La_5Ni_2Sn (the latter with the Cr_5B_3 structure type) are grown from reactions of Si or Sn in the La/Ni flux. If the iron content in the La/Fe/Al flux synthesis is low, the byproduct LaNiAl forms as hexagonal shaped rods; this is easily distinguishable

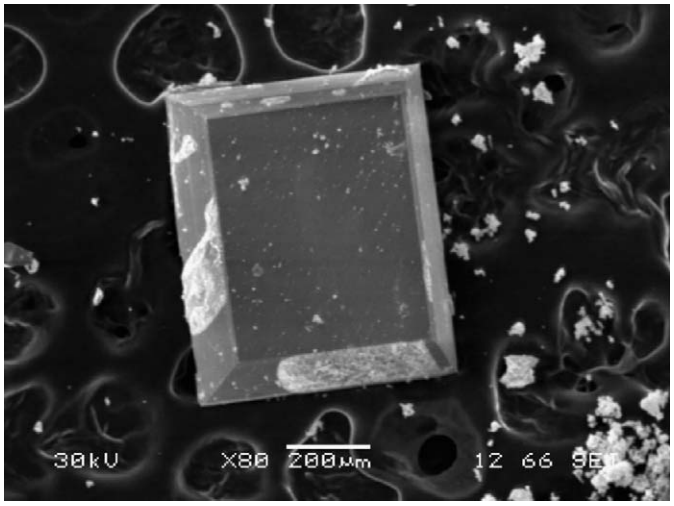

Fig. 2. SEM image displaying the typical plate-like morphology of $R_6T_{13-x}Al_xM_y$ crystals, viewed down the *c*-axis. The white powder is La_2O_3 from oxidation of excess La/Ni flux adhered to the surface after centrifugation.

from the $La_6Fe_{13-x}M_{1+x}$ phase which forms rectangular plates (see Fig. 2) [3,14].

Reactions of aluminum in a La/Fe eutectic (91.5/8.5 mol%; m.p. 780 °C) were also carried out to explore the synthesis of $La_6Fe_{13-x}Al_{1+x}$ in the absence of nickel. The higher melting point of the eutectic necessitated the use of higher soak temperatures (1050 °C) and a higher centrifugation temperature (815 °C). Instead of $La_6Fe_{13-x}Al_{1+x}$, these attempts yielded single crystals of the structurally related phase $LaFe_{13-x}Al_x$ with the cubic $NaZn_{13}$ structure type [14]. This raises the question of whether the nickel is required for the formation of $La_6Fe_{13-x}Al_{1+x}$, or if the use of higher reaction temperatures promotes the formation of a different phase. Nickel does not appear to be necessary to stabilize the formation of this structure; $Nd_6Fe_{13-x}Al_{1+x}$ can be grown in a Nd/Fe eutectic (*vide infra*) or a Nd/Al mixture [12]. It is possible that the tetragonal phase is stable with respect to the liquid at a specific temperature range. The growth of $LaFe_{13-x}Al_x$ from a higher temperature reaction may indicate that this phase is more thermodynamically stable then the $La_6Fe_{13-x}Al_{1+x}$ phase; the presence of nickel in the flux allows for the use of lower reaction temperatures, enabling isolation of the latter compound. Chan et al. have observed similar behavior in gallium flux; the phases Ce_2PdGa_{12} and $CePdGa_6$ form from identical reaction ratios by utilizing different heating profiles and centrifugation temperatures [15].

3.1.2. Manganese analogs

There have been several accounts of limited Mn doping into the cubic $LaT_{13-x}Al_x$ (T = Fe, Co) structure to yield phases such as $LaCo_{10}Mn_3$ and $LaFe_7Al_5Mn$ [16]. However, there are no reports of replacing Fe with Mn in the tetragonal $R_6Fe_{13-x}M_{1+x}$ compounds. Addition of manganese instead of iron to reactions in La/Ni flux successfully yielded ternary $La_6Mn_{13-x}Al_{1+x}$ and quaternary $La_6Mn_{13-x}Al_xM_y$ phases. An increase in both the *a*- and *c*-axis parameters is observed in going from $La_6Fe_{10}Al_4$ to $La_6Mn_{10}Al_4$ (Table 1). However, these systems are complicated by incorporation of nickel from the flux, confirmed by SEM–EDS analyses (scans of interiors of crystals indicate Ni substituting for Mn at levels ranging from 2% for $La_6Mn_{10}Al_4$ up to 30% for $La_6Mn_{10}Al_3Sb_{0.92}$). The preferred site of Ni incorporation could not be determined by X-ray diffraction. Another indication of Ni incorporation is seen during centrifugation; no noticeable removal of molten flux occurs, indicating a shift away from the low-melting eutectic ratio due to the reduction of the amount of nickel in the solution as the product crystallizes. Use of a La/Mn (83/17 mol%; m.p. 701 °C) eutectic was explored for growth of these phases without Ni impurities; these attempts have been unsuccessful. This, along with the absence of a pure (containing only manganese) cubic $LaMn_{13-x}Al_x$ phase, may indicate that transition metals with higher valence electron count are needed to stabilize the formation of manganese icosahedra in these structures.

3.1.3. Neodymium compounds

Single crystals of $R_6Fe_{13-x}Al_{1+x}$ phases with R = Nd were successfully grown using a Nd/Fe (79.5/20.5 mol%; Alfa Aesar) flux with a melting point of ~685 °C, using the same elemental ratios for the reactants as before. Each soak point in the heating profile was raised by 100 °C to accommodate the higher melting point of this flux. Cell volumes of ternary Al analogs $R_6Fe_{13-x}Al_{1+x}$ show a ~3.9% decrease in cell volume going from R = La to R = Nd. The dominant decrease in length occurs along the *c*-axis which is in good agreement with previously reported results [8,17]. Preliminary work on quaternary variants indicates that antimony can be incorporated into the 4*a* site to form $Nd_6Fe_{11.5}Al_{1.5}Sb_{0.5}$. Substitution of Mn for Fe was also explored in the Nd systems (by adding Mn to the Nd/Fe eutectic reactions). This results in an expansion in the unit cell as the larger Mn replaces Fe. Complete substitution was not achieved and accurate stoichiometries for $Nd_6(Fe/Mn)_{13-x}Al_{1+x}$ phases were difficult to determine. Elemental analysis using SEM–EDS was not reliable due to overlap of Mn and Fe peaks in the EDS spectra, and the electron density of the elements is too similar to distinguish in the X-ray diffraction data.

3.2. Structure description

The structure of $R_6Fe_{13-x}Al_xM_y$ (R = lanthanide, M = main group or late transition metal element) is shown in Fig. 1. The 2-D iron slabs (comprised of 4*d*, 16*k*, 16l_1, and 16l_2 sites) can be described as layers of linked icosahedral Fe clusters with Al mixing on the 16l_2 Fe site (outermost or capping site of the layer). Similar layers of linked icosahedra, and similar required Fe/Al mixing, can be seen in the cubic $LaFe_{13-x}Al_x$ ($1 \le x \le 7$); all the icosahedra are centered by iron, but the apices are occupied by a mixture of Fe/Al [18]. In tetragonal $R_6Fe_{13-x}Al_xM_y$ these iron slabs are separated by lanthanide layers (with atoms on 8*f* and 16*l* sites) centered by the 4*a* site containing a main group element.

3.2.1. The 4a site

In the ternary phase $La_6Fe_{10}Al_4$, the 4*a* site is occupied by aluminum. Restricting the amount of Al in the synthesis results in incorporation of Fe onto the 4*a* site. This can be confirmed by examining the occupation of the 4*a* site in numerous ternary analogs (see Table 1); in many cases, the XRD data indicate an electron density higher than Al itself. Refinement of this site as a mixture of Al and Fe indicates occupation in the range of 3–35% Fe. The presence of Fe on this site has not been previously reported and could contribute to the difficulty in understanding the magnetic properties of the system.

Occupation of the 4*a* site by different main group elements in the presence of Al readily occurs, producing the quaternary variants $La_6Fe_{13-x}Al_xM_y$ listed in Table 2. A wide variety of electronegative main group elements incorporate into this site, likely stabilized by the surrounding environment of electropositive lanthanum ions. We can confirm the incorporation of Pb, Bi, Sb, P, As, Ag, and Ge into the 4*a* site. Attempts at synthesizing analogs containing Sn and Te did not lead to any products.

Attempts to incorporate S, Se, Cu, and Au yielded single crystal products containing these elements (according to EDS) but the 4*a* site occupancy and the resulting stoichiometry is not clear due to the fact that partial occupancy of these elements produces similar electron density as an aluminum atom or a Fe/Al mixture. Stoichiometries in Table 2 are based on refinements with the 4*a* site partially occupied by the main group element. This manner of refinement produces the best agreement with elemental analysis results, and is also supported by electronegativity arguments. Also, some variation in occupancy can be induced by adjusting the stoichiometry of the reaction (*vide infra*). However, due to the semi-quantitative nature of EDS elemental analysis, it is not possible to rule out a M/Al or M/Fe/Al mixture on this site.

Occupation of the 4*a* site is affected by a number of variables, including the size of the *M* element, the reaction stoichiometry, and possibly the valence electron count. The size of the element *M* is a dominant factor. Analogs with smaller *M* (Al, P, and As) atoms readily achieve near 100% occupancy of this site. For larger elements on this site, occupation is affected by reaction ratio, with an excess of *M* in the flux needed to promote filling of the site. Three bismuth analogs $La_6Fe_{10}Al_3Bi_y$ were synthesized with bismuth reactant amounts of 30, 60, and 100 mg; resulting occupations of the 4*a* site were 47%, 75%, and 91%, respectively (see Table 2). Increased occupation of the 4*a* site with Bi results in an increase in the *c*-axis parameter. Higher *c*-axis parameters are also observed for analogs containing other large main group elements. These elements expand the packing of the La layer whereas smaller *M* elements like Al, P, and S cause much smaller perturbations.

3.2.2. *The* Fe/Al *mixed* $16l_2$ *site*

The $16l_2$ Fe/Al mixed site is the outermost, capping site of the iron layers. The five neighboring La atoms distort the local environment and enforce a greater volume, which promotes accommodation of the larger Al atom (143 pm) compared to Fe (126 pm). The $16l_2$ site incorporates only iron and aluminum even in the presence of other main group elements. The Fe/Al ratio can be controlled by changing the synthesis ratio; surprisingly, it is also affected by adjusting the maximum dwell temperature. With a 1|1.5|0.5 mmol ratio of La|Fe|Al in 1 g of La/Ni flux, dwell temperatures of 1000, 1050, and 1100 °C result in the Fe content on the $16l_2$ site increasing from 23% to 24% and 27%, respectively. By varying *both* the soak temperature and molar amounts of Al added we were able to synthesize analogs with Fe in the range of 9–40% incorporation on this site. Higher amounts of iron in this site are seen for the $Nd_6Fe_{13-x}Al_xM_y$ phases grown from the iron-rich Nd/Fe eutectic. While occupancy of the 4*a* site primarily affects the *c*-axis, the Fe/Al ratio on site $16l_2$ seems to have a larger affect on the *a*-axis of the unit cell. On average, the *a*-axis decreases as the iron content on the $16l_2$ mixed site increases. This is in agreement with the smaller radius of iron compared to aluminum. This formation of a more compact iron slab with associated shorter Fe–Fe distances has a strong impact on the magnetic properties of these compounds.

3.3. *Magnetic properties*

The magnetic properties of $R_6Fe_{13-x}M_{1+x}$ (R = La, Pr, Ce, Nd) compounds have been studied by a variety of groups [4–6,8,9,12,19,20]. Initially there was a large disparity in the proposed magnetic ordering properties with antiferromagnetism, ferrimagnetism, and ferromagnetism all being reported [21–23]. However, some of these conflicting models were based on data from polycrystalline samples with traces of ferromagnetic R_2Fe_{17} and α-Fe impurities. The most consistently reported low temperature magnetic structure model consists of alternating ferromagnetic (FM) slabs of Fe and *R* with an antiferromagnetic (AF) translation (Type II) occurring across the 4*a* site along the *c*-axis [12,24,25]. This leads to three separate intralayer ordering mechanisms, FM Fe–Fe, FM *R*–Fe, and FM *R*–*R* and two competing interlayer ordering mechanisms across the 4*a* site, AF *R*–*M*–*R* and FM *R*–*M*–*R* with an already present AF iron lattice. Study of the lanthanum analog eliminates the *R*–Fe and *R*–*R* magnetic ordering and allows isolation of the FM intralayer Fe–Fe coupling and the AF ordering between the Fe layers.

3.3.1. $La_6Fe_{13-x}Al_{1+x}$

Magnetic measurements on $La_6Fe_{10.25}Al_{3.75}$ were performed with the field parallel and then perpendicular to the *c*-axis of the material. With diamagnetic La^{3+} cations, the type II antiferromagnetic coupling between ferromagnetic Fe slabs is maintained; the data in Fig. 3 show an antiferromagnetic transition at a T_N of ~115 K. Below the Neel temperature, the spins are aligned along the *c*-axis. Application of higher fields (~1–3 T; see Supplementary Material) causes the transition to broaden and shift to lower temperatures; the AF transition disappears at fields above 3 T, yielding data typical of a saturated ferromagnet. This is also indicated in the magnetization data taken at 1.8 K (Fig. 4). A metamagnetic transition is apparent when a field of 3 T is applied

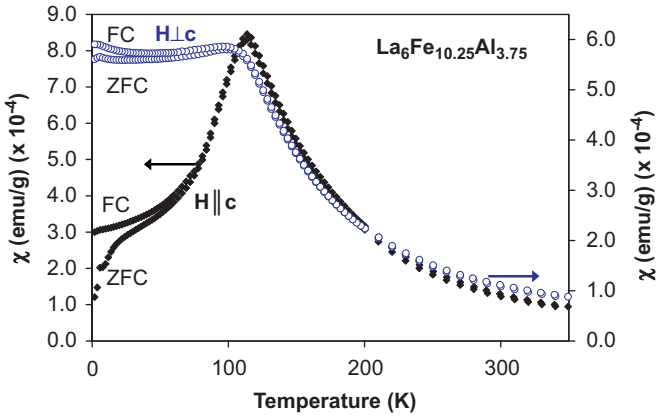

Fig. 3. Susceptibility measurements (field cooled and zero-field cooled) for $La_6Fe_{10.25}Al_{3.75}$ with the 0.2 T field applied parallel to the *c*-axis (filled symbols, primary axis) and perpendicular to the *c*-axis (open symbols, secondary axis).

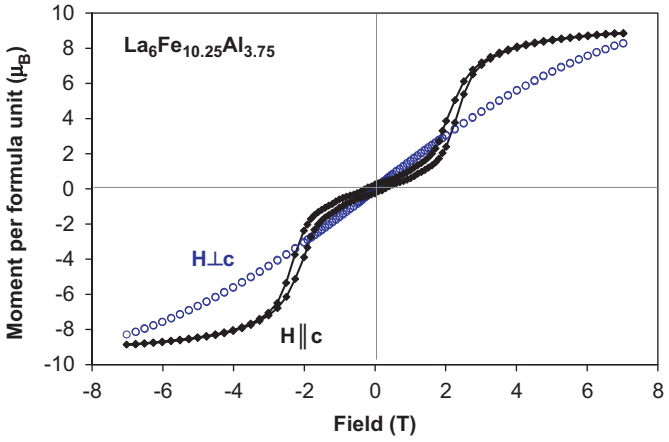

Fig. 4. Magnetization measurements for $La_6Fe_{10.25}Al_{3.75}$ at 1.8 K; measurements taken with the field applied parallel to the *c*-axis (filled symbols) and then perpendicular to the *c*-axis (open symbols).

along the *c*-axis; the layers of iron atoms with spins oriented in opposition to the applied field rotate their magnetic moments to align with the field, yielding an overall ferromagnetic state. There are slight discrepancies between the field-cooled and zero-field cooled susceptibility data below the antiferromagnetic transition (Fig. 3). This FC/ZFC splitting only occurs in fields less then ~2 T. It is possibly due to the disorder in the Fe/Al mixed sites in each layer, leaving a residual number of uncancelled spins below T_N which cause spin glass behavior. This is also indicated in the slight hysteresis in the magnetization data (Fig. 4) at fields below 3 T. At higher fields the material orders ferromagnetically, eliminating any spin frustration, so no hysteresis is evident at fields above 3 T.

Above the AF transition, the susceptibility does not fit to Curie-Weiss behavior for paramagnetic materials, although the temperature dependence of the inverse susceptibility does approach linearity at the highest temperature range measured. An approximate fit of this region yields an average moment per iron atom of 1.45 μ_B and a positive Weiss constant ($\theta = 157$ K), indicative of FM interactions between iron atoms. These data indicate that the compound does not achieve a fully paramagnetic state at the temperatures available in this study. This is borne out by heat capacity measurements; see Fig. 5. Subtle anomalies and a change in slope of the heat capacity temperature dependence are observed near the AF transition temperature. However, more notable are the fluctuations observed above 200 K in data taken at both 0 and 1 T. This behavior may be indicative of long range FM ordering within the iron slabs breaking up into short range FM ordering of spin clusters above the Neel temperature, which gradually randomize as the temperature rises until the fully paramagnetic state is reached at temperatures above those available in the susceptibility study [26].

The magnetic behavior of several of the $La_6Fe_{13-x}Al_xM_y$ quaternary phases was also studied. All of the compounds studied show a similar type II antiferromagnetic transition with T_N varying from 110 to 175 K (see Supplementary Material). Analogs with $M =$ Cu, Pb, and Se have the highest transition temperature (T_N above 150 K); lower transition temperatures are seen for $M =$ Bi and S analogs. The nature of the M element and its occupancy on the 4*a* site does not seem to be a crucial factor. Instead, it appears that the Fe/Al ratio on the $16l_2$ site is the important parameter; analogs with high T_N have higher Fe content on this site (see Table 2). Our observed values of T_N are positioned within the range reported by Jonen et al. ($La_6Fe_9Al_5$ and $La_6Fe_{11}Al_3$ have Neel temperatures of 100 and 230 K, respectively) [17]. As mentioned previously, increasing the iron content leads to a shorter *a*-axis and stronger intralayer Fe–Fe interactions. Shorter Fe–Fe bonds leading to improved exchange coupling and therefore a higher ordering temperature is observed in several other iron-rich systems [27]. This can also be viewed in terms of an itinerant electron magnetism model, in which the 3d bands are split into majority and minority spin sub-bands with the latter higher in energy in an applied field. The relative position of these sub-bands shift with changes in the Fermi energy level [28]. Variation of electron count (as will occur with changing Fe/Al ratio) will therefore affect the strength of the magnetic coupling between iron atoms.

3.3.2. $Nd_6Fe_{13-x}Al_{1+x}$

The $Nd_6Fe_{10.5}Al_{3.5}$ analog exhibits the same type II antiferromagnetic ordering of the iron slabs seen in the lanthanum phase, but additional transitions are seen at lower temperatures due to ordering of the Nd sublattices. The antiferromagnetic transition of the iron slabs occurs at 232 K (see Fig. 6). This is considerably higher than the T_N of the lanthanide analogs studied here, likely due to the much higher Fe/Al ratio on the $16l_2$ site of the Nd phase (grown from Nd/Fe eutectic, a much more iron-rich environment than the La/Ni eutectic). The orientation dependence of the susceptibility indicates that the Fe moments align predominantly along the *c*-axis. This is in agreement with the data observed by Dennis et al. and also with the neutron diffraction results reported by Buschow, although the latter reported a slight canting ($<12^\circ$) from the *c*-axis [8,12]. The transition at 77 K is due to ordering of the neodymium moments, which again appear to be aligned predominantly along the *c*-axis. Below this temperature, separation of FC and ZFC behavior is observed. This might indicate spin glass behavior caused by Fe/Al mixed sites, or it may be a result of spin canting. Neutron studies indicate that the canting angle of the spins varies with temperature, with changes being particularly abrupt below 33 K; our data show complex behavior below 30 K which may be related to canting variations [8]. The temperature dependent susceptibility on isotropic powders reported by Jonen et al. [17], with transitions seen at 225, 70, and 20 K, looks suitably like an averaging of the orientation dependent data shown in Fig. 6.

Field dependent measurements of magnetization at 1.8 K (Fig. 7) display several hysteretic metamagnetic transitions, strongly dependent on orientation. Magnetization at 10 K was previously reported for Nd/Al grown crystals oriented with field parallel to the *c*-axis; a similar hysteresis was seen, but the small steps in the loop were not observed at that temperature [12]. Magnetization data taken on a powdered sample at 0.6 K reveal

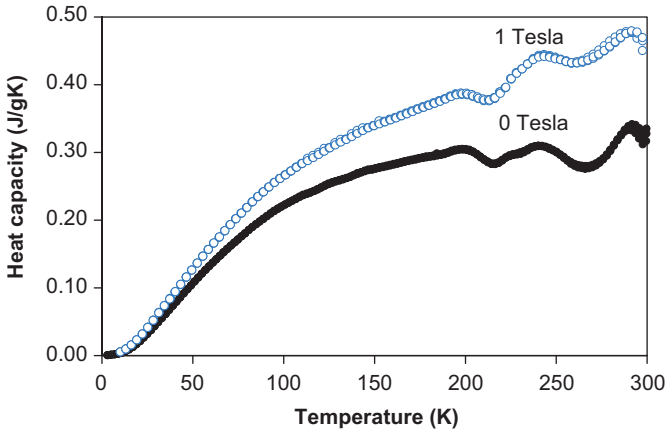

Fig. 5. Heat capacity measurements of $La_6Fe_{10.25}Al_{3.75}$. Sharp fluctuations near 300 K are from grease used to adhere crystals to the PPMS measurement puck.

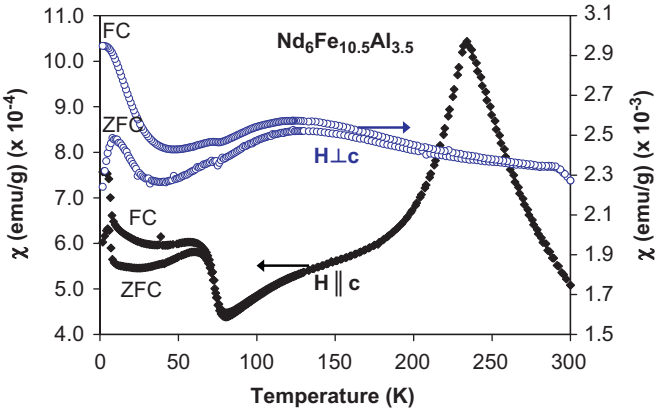

Fig. 6. Susceptibility measurements (FC and ZFC) for $Nd_6Fe_{10.5}Al_{3.5}$ with the 0.2 T field applied parallel to the *c*-axis (filled symbols, primary axis) and perpendicular to the *c*-axis (open symbols, secondary axis).

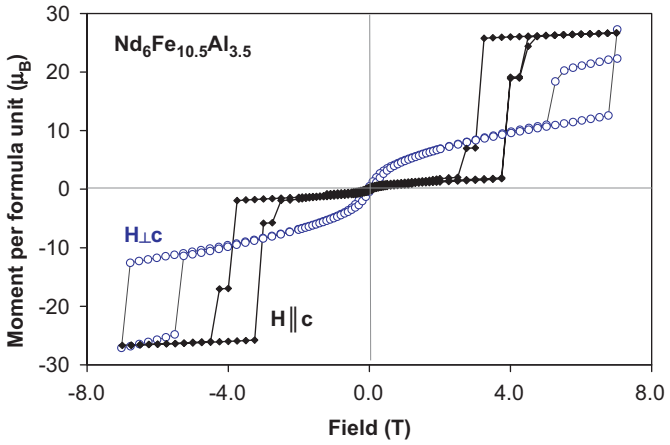

Fig. 7. Magnetization measurements for $Nd_6Fe_{10.5}Al_{3.5}$ at 1.8 K; measurements taken with the field applied parallel to the *c*-axis (filled symbols) and then perpendicular to the *c*-axis (open symbols).

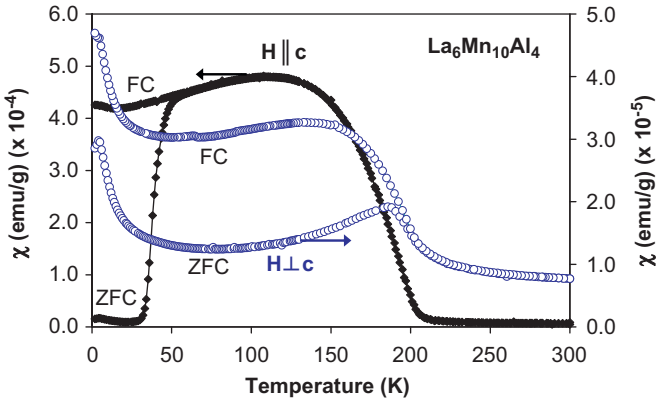

Fig. 8. Susceptibility measurements (FC and ZFC) for $La_6Mn_{10}Al_4$ with the 0.2 T field applied parallel to the *c*-axis (filled symbols, primary axis) and perpendicular to the *c*-axis (open symbols, secondary axis).

several steps in their hysteresis loop [17]. As the temperature is lowered, additional distinct spin orientations stabilize at different fields, resulting in more metamagnetic transitions to spin arrangements at different canting angles. This is supported by our observation of hysteresis loops at fields above 5 T in the data collected on a crystal oriented with the field perpendicular to the *c*-axis; this has not been reported before. Due to the complex nature of these systems proposing an exact magnetic ordering model is difficult; the large single crystals of $Nd_6Fe_{13-x}Al_{1+x}$ which can be grown in Nd/Fe flux may facilitate future studies to clarify this issue.

3.3.3. $La_6Mn_{13-x}Al_{1+x}$

Substitution of iron with manganese in the La/Ni flux syntheses yields $La_6Mn_{10}Al_4$; EDS indicates 2% nickel incorporation, presumably in the manganese layer. This phase displays strong ferromagnetic behavior (T_C~200 K, coercive field = 1 T) with the easy axis of magnetization parallel to the *c*-axis; see Figs. 8 and 9. This is somewhat surprising, since manganese-rich intermetallics often feature non-magnetic or antiferromagnetic Mn. Previous studies indicate that for compounds with Mn–Mn distances below 2.67 Å, the Mn moments are not stable [29]; these bond lengths in $La_6Mn_{10}Al_4$ are all below this threshold. However, the incorporation of aluminum and nickel into the manganese layers acts to cut the 3d–3d bonds between Mn atoms; this will cause the Mn 3d band to become narrower and the Mn moment to become stable [30]. This would facilitate magnetic ordering and allow for the observed large coercivity. While the siting of Ni and Mn cannot be distinguished in the XRD structure solution of the compounds studied here, XAFS studies on manganese-substituted cubic $LaCo_{13-x}Mn_x$ indicates that manganese atoms are preferentially located at the corners of the icosahedra whereas cobalt prefers the center site [16]. If similar preferences are exhibited for this tetragonal structure, the manganese atoms will be interspersed by nickel atoms centering the icosahedra and aluminum atoms on the $16l_2$ capping sites of the manganese layer. This would allow the Mn moments to be retained. The moments on the manganese atoms do appear to be small, as seen by the low value of the saturation magnetization (Fig. 9).

Significant differences are seen in the field-cooled and zero-field cooled susceptibility data in Fig. 8. The mixing of nickel and aluminum on some of the manganese sites could contribute to the spin disorder for both orientations of the crystal, similar to that seen in the $La_6Fe_{13-x}Al_{1+x}$ phases. However, this FC/ZFC splitting is

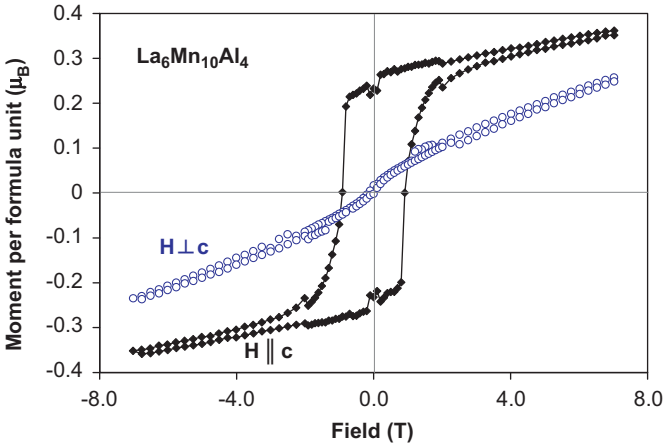

Fig. 9. Magnetization data for $La_6Mn_{10}Al_4$ collected at 1.8 K with the field applied parallel to the *c*-axis (filled symbols) and then perpendicular to the *c*-axis (open symbols).

more likely to be an artifact from the centering process. Ferromagnetic compounds with large coercivity are strongly affected by the magnetic fields used during the sample centering process and the slight magnetic fields present in the SQUID when the field is set for zero magnetic field [31]. Therefore these samples are not cooled under ideal zero-field conditions; this is the likely source of the very large differences in the ZFC and FC susceptibilities.

4. Conclusion

Lanthanide/late transition metal eutectic mixtures have proven to be a very useful synthesis medium for polar intermetallics. Large crystals of a wide variety of ternary $R_6T_{13-x}Al_{1+x}$ (T = Fe, Mn; R = La, Nd) and quaternary $R_6T_{13-x}Al_xM_y$ compounds can be grown, allowing for the collection of orientation dependent magnetic susceptibility data which can be combined with future neutron diffraction studies to achieve a clearer understanding of the magnetic properties of these phases. The substitution of iron with manganese to yield a ternary $La_6Mn_{13-x}Al_{1+x}$ analog is of particular interest, as Mn-rich variants of this structure and the strong ferromagnetism exhibited by the compound have not been previously reported.

Supplementary material

Additional magnetic susceptibility data of several $La_6Fe_{13-x}Al_xM_y$ analogs and susceptibility data taken at different applied fields.

Acknowledgments

We thank Nathanial Falb for his assistance with synthesis. We thank Dr. Michael Shatruk for many useful discussions about the magnetic properties, Vasanth Ramachandran for his help with the SQUID and PPMS measurements and Dr. Eric Lochner for his assistance with the instruments at the MARTECH facilities. This research was supported by the FSU Department of Chemistry and Biochemistry and the National Science Foundation (Grant number DMR-05-47791).

Appendix A. Supplementary material

Supplementary data associated with this article can be found in the online version at 10.1016/j.jssc.2009.08.011.

References

[1] T.B. Massalski, H. Okamoto, Binary Alloy Phase Diagrams, second ed., ASM International, Materials Park, OH, 1990.
[2] M.G. Kanatzidis, R. Pottgen, W. Jeitschko, Angew. Chem. Int. Ed. 44 (2005) 6996–7023;
Z. Fisk, J.P. Remeika, in: S. Gschneider, S. Eyring (Eds.), Handbook on the Physics and Chemistry of Rare Earths, vol. 12, Elsevier Science, Amsterdam, 1989 (Chapter 81);
Z. Fisk, P.C. Canfield, Philos. Mag. 65 (1992) 1117–1123.
[3] E. Benbow, Ph.D. Dissertation, Florida State University, 2008.
[4] F.W. Wang, P.L. Zhang, B.G. Shen, Q.W. Yan, Chinese Phys. 13 (2004) 918–923.
[5] C.H. de Groot, K.H.J. Buschow, F.R. de Boer, Phys. Rev. B 57 (1998) 11472–11482.
[6] S.J. Kennedy, E. Wu, F.W. Wang, P.L. Zhang, Q.W. Yan, Physica B 276 (2000) 622–623.
[7] P. Schrey, M. Velicescu, J. Magn. Magn. Mater. 101 (1991) 417;
T. Kajitani, K. Nagayama, T. Umeda, J. Magn. Magn. Mater. 117 (1992) 379–386.
[8] P. Schobinger-Papamantellos, C. Ritter, K.H.J. Buschow, J. Magn. Magn. Mater. 260 (2003) 156–172.
[9] P. Schobinger-Papamantellos, K.H.J. Buschow, C.H. de Groot, F.R. de Boer, C. Ritter, J. Magn. Magn. Mater. 218 (2000) 31–41.
[10] SAINT, Version 6.02a, Bruker AXS, Inc., Madison, WI, 2000.
[11] G.M. Sheldrick, SHELXTL NT/2000, Version 6.1, Bruker AXS, Inc., Madison, WI, 2000.
[12] R.W. McCallum, I.R. Fisher, N.E. Anderson, P.C. Canfield, M.J. Kramer, K.W. Dennis, IEEE Trans. Magn. 37 (2001) 2147–2149.
[13] E. Benbow, N.S. Dalal, S.E. Latturner, J. Am. Chem. Soc. 131 (2009) 3349–3354.
[14] P. Villars, L.D. Calvert, Pearson's Handbook—Crystallographic Data for Intermetallic Phases, ASM International, Materials Park, OH, 1998.
[15] R.T. Macaluso, J.N. Millican, S. Nakatsuji, H.O. Lee, B. Carter, N.O. Moreno, Z. Fisk, J.Y. Chan, J. Solid State Chem. 178 (2005) 3547–3553.
[16] Y. Guo, J. Liang, X. Zhang, W. Tang, Y. Zhao, G. Rao, J. Alloys Compd. 257 (1997) 69–74;
K. Asada, K. Konno, M. Matsuura, M. Sakuri, A. Fujita, K. Fukamichi, J. Alloys Compd. 350 (2003) 47–51.
[17] S. Johen, H.R. Rechenberg, J. Campo, J. Magn. Magn. Mater. 242–245 (2002) 803–805.
[18] R.B. Helmholdt, T.T.M. Palstra, G.J. Nieuwenhuys, J.A. Mydosh, A.M. van der Kraan, K.H.J. Buschow, Phys. Rev. B 34 (1986) 169.
[19] F. Grandjean, G.J. Long, M. Guillot, O. Isnard, K.H.J. Buschow, J. Phys.: Condens. Matter. 16 (2004) 4347–4355.
[20] F. Wang, P. Zhang, B. Shen, Q. Yan, H. Gong, J. Appl. Phys. 87 (2000) 6043–6045.
[21] C.H. de Groot, F.R. de Boer, K.H.J. Buschow, D. Hautot, G.J. Long, F. Grandjean, J. Alloys Compd. 233 (1996) 161–164.
[22] Q.W. Yan, P.L. Zhang, X.D. Sun, B.P. Hu, Y.Z. Wang, X.L. Rao, G.C. Liu, C. Gou, D.F. Chen, Y.F. Cheng, J. Phys. Condens. Matter 6 (1994) 3101–3107.
[23] F. Weizter, A. Leithe-Jasper, P. Rogl, K. Hiebl, A. Rainbacher, G. Wiesinger, W. Steiner, J. Friedl, F.E. Wagner, J. Appl. Phys. 75 (1994) 7745–7751.
[24] O. Isnard, G.J. Long, D. Hautot, K.H.J. Buschow, F. Grandjean, J. Phys. Condens. Matter 14 (2002) 12391–12409.
[25] P. Schobinger-Papamantellos, K.H.J. Buschow, C. Ritter, J. Alloys Compd. 359 (2003) 10–21.
[26] F. Wang, J. Wang, P. Zhang, B. Shen, Q. Yan, L. Zhang, Physica B 269 (1999) 17–21.
[27] W.E. Wallace, Prog. Solid State Chem. 16 (1985) 127;
A. Szytula, J. Leciejewicz, CRC Handbook of Crystal Structures and Magnetic Properties of Rare Earth Intermetallics, CRC Press, Boca Raton, 1994.
[28] K.H.J. Buschow, F.R. de Boer, Physics of Magnetism and Magnetic Materials, Kluwer Academic Publishers, New York, 2003.
[29] H. Wada, H. Nakamura, K. Yoshimura, M. Shiga, Y. Nakamura, J. Magn. Magn. Mater. 70 (1987) 134.
[30] M. Coldea, M. Neumann, S. Lutkehoff, S. Mahl, R. Coldea, J. Alloys Compd. 278 (1998) 72–79;
W. Suski, B. Belan, T. Mydlarz, K. Wochowski, J. Alloys Compd. 367 (2004) 215–218.
[31] P.A. Joy, P.S. Anil Kumar, S.K. Date, J. Phys. Condens. Matter 10 (1998) 11049–11054.